Cellulose (2024) 31:1875–1890
https://doi.org/10.1007/s10570-023-05680-0

ORIGINAL RESEARCH

Localization and characterisation of brown rot in two types of acetylated wood

Andrea Ponzecchi · Gry Alfredsen · Maria Fredriksson · Emil E. Thybring · Lisbeth G. Thygesen

Received: 6 September 2023 / Accepted: 3 December 2023 / Published online: 10 January 2024

Abstract Acetylation is a commercialised chemical wood modification technology that increases the durability of wood against microbial attack. However, the details of how acetylation protects the wood structure from fungal degradation are still unclear. In this study, we tested the hypothesis that the resistance against microbial attack depends on the localisation of acetylation within the cell wall. The methodology involved two types of acetylation (uniform and lumen interface modification), which were analysed by lab-scale degradation with *Rhodonia placenta*, chitin quantification, infrared spectroscopy, and Raman microspectroscopy. The location of the acetylation did not affect overall mass loss during degradation experiments. Instead, the mass loss was related to the intensity of the treatment. However, chemical imaging of the interface acetylated specimens showed that degradation primarily took place in cell wall regions that were less acetylated. It was also observed that the fungus required more fungal biomass (i.e., fungal mycelia) to degrade acetylated wood than untreated wood. Based on dimensions and comparison to a reference spectrum, several cross-sections of hyphae located within lumina were discovered in the Raman images. These hyphae showed presence of chitin, water and chelated metals within their walls, and could be separated into an inner and an outer part based on their chemistry as seen in the spectra. The outer part was distinguished by a relatively higher amount of water and less chelated iron than the inner part.

Keywords Wood · Acetylation · Degradation · Spectroscopy · Holocellulose

Supplementary Information The online version contains supplementary material available at https://doi.org/10.1007/s10570-023-05680-0.

A. Ponzecchi (✉) · E. E. Thybring · L. G. Thygesen
Bioresource Chemistry and Technology, Department of Geoscience and Natural Resource Management, University of Copenhagen, Frederiksberg, Denmark
e-mail: apo@ign.ku.dk

G. Alfredsen
Department of Wood Technology, Norwegian Institute of Bioeconomy Research, Ås, Norway

M. Fredriksson
Division of Building Materials, Lund University, Lund, Sweden

Introduction

Wood possesses several appealing characteristics as a construction material, including the ability to store carbon while in use and its visual appeal as a natural material. However, wood is vulnerable to damage from wood-degrading organisms when used in construction (Daniel 2016). Wood is prone to fungal degradation if exposed to moist environments, leading to significant strength loss and reduced service life (Schultze-Dewitz 1966), especially when brown

rot fungi are involved (Arantes and Goodell 2014; Wagner et al. 2015). Previous studies indicate that this group of fungi break down the cell walls of wood in a two-stage mechanism comprising initial oxidative processes followed by enzymatic activity (Daniel 2016; Schilling et al. 2013; Zhang et al. 2016), resulting in depolymerisation of mainly cellulose and hemicelluloses and modification of lignin (Arantes et al. 2011; Daniel 2016; Durmaz et al. 2016; Yelle et al. 2011).

Several wood modification technologies (i.e., wood protection systems with non-biocidal mode of action) have been developed to enhance the durability of wood (Hill 2006; Rowell 1983). Among these, acetylation has been commercialized (Mantanis 2017; Zelinka et al. 2022). Acetylation improves wood durability by replacing hydroxyl groups with acetyl esters within wood cell walls, thereby reducing the space available for water (Mantanis 2017). Reducing the equilibrium moisture content to less than 0.23–0.25 g/g appears to effectively prevent decay in modified wood (Thybring 2013; Williams and Hale 2003). This is likely because water is needed by the wood degrading fungi for transport purposes to and from the hyphae located in the cell lumina, but water is also used to form hydrated minerals such as oxalates, a known byproduct of fungal depolymerization of wood cell walls (Arantes and Goodell 2014; Gadd 1999; Gadd et al. 2014; Guggiari et al. 2011). Nonetheless, recent results suggest that even highly acetylated wood can be degraded after sufficient time under optimal moisture conditions (Beck et al. 2018b; Thygesen et al. 2021). Gene expression studies have shown that brown rot fungi are able to do so by upregulating and prolonging the oxidative stage when degrading acetylated wood (Beck et al. 2018).

Here we tested the hypothesis that not only the extent of acetylation, but also how it is distributed within the wood cell wall affects how brown rot fungal degradation plays out on the nm to µm scale. To this end, we included both uniformly acetylated wood and wood subjected to targeted acetylation where only the lumen-cell wall interface was acetylated (Digaitis et al. 2021). This model substrate is interesting because it shows how the fungus reacts to the situation where the central S2 layer remains (partially) untreated, while the cell wall material closest to the hyphae in the cell lumen is heavily acetylated.

Materials and methods

Wood samples and acetylation

Wood blocks of $5 \times 5 \times 10$ (longitudinal) mm^3 Norway spruce sapwood (*Picea abies* (L.) Karst) were obtained from an experimental forest in northern Sweden, see Fredriksson et al. (2016) for more information. 512 blocks were used in total for this study, equally divided into four batches of wood material: untreated and three types of acetylation.

- The acetylated samples were modified as in Digaitis et al. (2021), using acetic anhydride (99.3%, VWR Chemicals, Radnor, PA, USA) and pyridine (Sigma Aldrich, Merck KGaA, Darmstadt, Germany) following two different protocols to either modify the cell wall uniformly, or the interface between cell walls and cell lumina.
- Prior to acetylation, all specimens were dried for 24 h at 60 °C in a vacuum oven and subsequently weighed. Following the acetylation procedure, the specimens were dried once more at 60 °C for 24 h under vacuum, after which their mass was re-measured. The dry mass before and after modification was compared to determine the degree of modification (R_{mod}):

$$R_{mod}\ (g/g) = \frac{m_{dry} - m_{dry,0}}{m_{dry,0}} \quad (1)$$

- where $m_{dry,0}$ (g) and m_{dry} (g) are the dry masses before and after modification, respectively.
- Independent of the treatment, 10 g of reagent solution was used for each gram of dry wood. A detailed and complete protocol can be found in Digaitis et al. (2021).
- Specifically:
- UNIFORM HIGH: 128 blocks impregnated with a 1:4 mixture (v/v) of acetic anhydride and pyridine were held at 80 °C for 180 min, obtaining uniformly acetylated samples with $R_{mod} = 0.224 \pm 0.006$ g/g
- UNIFORM LOW: 128 blocks impregnated with a 1:4 mixture (v/v) of acetic anhydride and pyridine were held at 80 °C for 20 min, obtaining uniformly acetylated samples with $R_{mod} = 0.155 \pm 0.008$ g/g

- INTERFACE: 128 blocks impregnated with pure acetic anhydride were held at 75 °C for 24 h, obtaining interface acetylated samples with R_{mod} = 0.096 ± 0.009 g/g.
- The use of pure acetic anhydride resulted in acetylation of cell wall-lumen interfaces only (INTERFACE), while the addition of pyridine promoted swelling, which facilitated the diffusion of acetic anhydride and ensured uniform acetylation of wood cell walls (UNIFORM) (Digaitis et al. 2021; Mantanis et al. 1994). All the samples were leached according to the European standard EN 84 (CEN 1997) before the decay test.

Wood decay in a controlled laboratory environment

Rhodonia (Postia) placenta FPRL 280 (Fr.) Niemelä, K.H. Larss. & Schigel was used for the decay test. Fungal monoculture inoculation followed the method used in Thygesen et al. (2021). Briefly described, the fungus was initially grown on 4% malt agar medium and then transferred to a liquid culture containing 4% malt. After two weeks, the liquid culture was homogenized and used to inoculate the samples. Petri dishes were filled with sterile soil adjusted to 95% of the soil's water-holding capacity, and the wood samples were placed on top of the soil with a sterilized plastic mesh in between wood and soil. Each sample was inoculated by pipetting 300 µL of the fungal suspension on top of the sample. The samples were incubated at 22 °C and 70% relative humidity until harvested. Every third week the mass of the dishes was measured, and sterile water was added to the soil to ensure stable moisture conditions throughout the experiment.

For untreated wood, 8 samples were harvested every week up to 6 weeks, with two harvests in the first week, yielding a total of 56 samples. For acetylated wood, 8 samples were harvested every week for the UNIFORM LOW and INTERFACE samples up to 15 weeks and every third week up to 45 weeks for UNIFORM HIGH samples. Thus, a total of 120 samples were harvested for each type of acetylated wood, as detailed in Table 1.

Three of the eight samples from each treatment and each harvesting point were vacuum dried at 60 °C for 24 h in order to determine the mass loss from fungal degradation. Mass losses were not corrected for acetylation mass gain. The remaining five samples were wrapped individually in aluminum foil and put directly into a container with liquid nitrogen. The samples were then stored at − 80 °C.

Specimens with mass loss above 15% were selected, when possible, for the spectroscopic analyses. The mass loss and harvest time of the samples subjected to the aforementioned analyses are highlighted in Fig. 1 and described in Tables S1.

Chitin monomer analysis

The chitin content was indirectly quantified by analysing monomer content (i.e., glucosamine after acid hydrolysis) by analyzing specimens with increasing levels of mass loss. 13 UNIFORM HIGH samples, 13 UNIFORM LOW, 16 INTERFACE and 11 UNTREATED samples were employed for this analysis, as depicted in Sect. 3.1.2 and in Fig. S1. The amount of chitin present in the degraded specimens was measured as an indicator of fungal biomass, according to the protocol described by Eikenes et al. (2005), including online fluorimetric o-phthalaldehyde derivatisation using a HPLC linked to a fluorescence detector (HPLC-FL).

Table 1 Average degree of modification (R_{mod}), harvest interval, maximum harvest time and number of samples employed for brown rot fungal degradation, for each type of wood material

Material	R_{mod} (g/g)	Total no of samples harvested	Harvest interval (weeks)	Maximum harvest time (weeks)
UNTREATED	0	56	1 (+ after 4 days)	6
UNIFORM HIGH	0.225 ± 0.006	120	3	45
UNIFORM LOW	0.155 ± 0.008	120	1	15
INTERFACE	0.096 ± 0.009	120	1	15

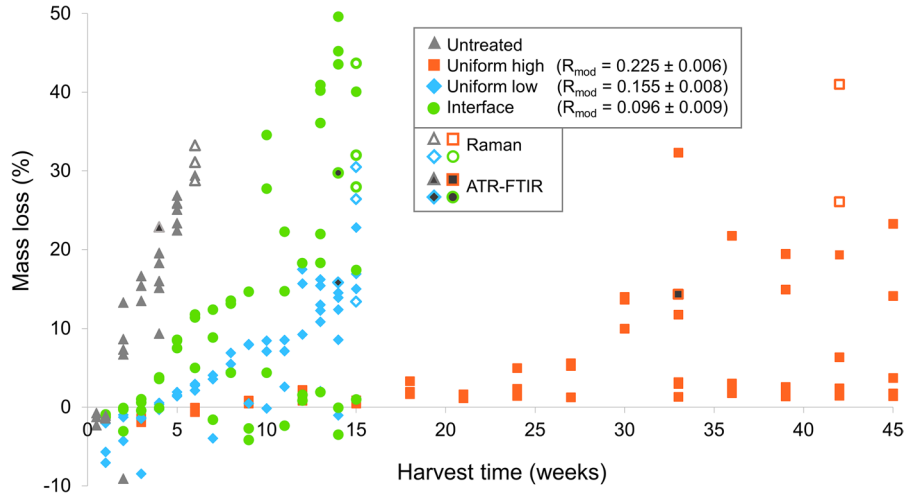

Fig. 1 Mass loss of the brown rot degraded spruce samples at different harvest times after incubation. The empty icons show samples studied by Raman micro-spectroscopy (Raman), while dark filled icons are samples studied by infrared spectroscopy (ATR-FTIR)

Attenuated total reflectance Fourier transform infrared (ATR-FTIR) spectroscopy

Infrared spectroscopy was used to investigate the bulk chemical changes in the wood samples. The wood samples, both acetylated and unmodified, were dried in a vacuum oven for 18 h at 60 °C to determine individual mass loss. Two thin cross-sections were cut from each dried specimen using a razor blade and allowed to acclimate in the laboratory environment for 72 h before being used for infrared measurements. Three replicate spectra were taken for each cross-section, and the mass loss data for each sample is provided in Table S1. The infrared measurements were conducted using a Nicolet 6700 FT-IR spectrometer (Thermo Scientific, Waltham, MA, USA) equipped with a Pike Technologies GladiATR diamond ATR. The spectra were obtained as the averages of 64 scans (128 for background) using a resolution of 4 cm^{-1} and a spectral range of 3800 – 400 cm^{-1}. MATLAB (version 2021a, MathWorks, Natick, MA, USA) was used for spectral analysis. The spectral ranges between 400 and 790 cm^{-1}, and between 1900 and 2500 cm^{-1}, were removed as they did not contain any relevant information about the wood samples. Linear baselines were applied to each absorbance peak, and three characteristic absorbance bands were chosen for analysis: the 1508 cm^{-1} band, which represents lignin with no carbohydrate contribution (Faix 1991), the 1107 cm^{-1} band, which is attributed to holocellulose (Schwanninger et al. 2004), and the 1732 cm^{-1} band, which is attributed to acetylation as well as hemicellulose as it is assigned to unconjugated C = O valence vibration of acetyl groups and C = O stretch in unconjugated ketones, carbonyls, and ester groups (Faix 1991). The 1107 cm^{-1} absorption is expected to contain information on both hemicellulose and cellulose, while the 1508 cm^{-1} absorbance is expected to remain relatively constant throughout the decay period, as the aromatic rings in lignin are thought to be the least affected structure of the wood cell wall degraded by brown rot fungi, albeit lignin modification does take place (Beck et al. 2018b; Füchtner and Thygesen 2023).

Raman micro-spectroscopy

To examine the chemical changes within wood cell walls, Raman micro-spectroscopy (Raman) was employed. Six specimens, each from acetylated and unmodified wood, were vacuum-oven dried for 18 h at 60 °C, and vacuum-saturated with deuterium oxide (99.98%, D_2O, Sigma-Aldrich, Munich, Germany). Three of the six specimens were pristine wood, while three where degraded. The mass loss data for unmodified and acetylated samples employed for this method is provided in Table S1. Using a cryotome (CM3050S, Leica Biosystems, Wetzlar, Germany) and following the protocol from Gierlinger et al. (2012), except for the use of D_2O instead of H_2O, two 20 µm cross-sections were produced from each specimen. The samples were then mounted in D_2O, covered with a borosilicate glass slide (thickness #1), and sealed with nail polish. Raman scans of

one full tracheid were taken from each wood cross-section utilizing a confocal Raman microscope (alpha 300R, WITec GmbH, Ulm, Germany) equipped with a UHTS 300 spectrometer and a 100x oil immersion objective (Zeiss "NAchroplan," NA = 1.2, transmittance 73%, Carl Zeiss GmbH, Jena, Germany). A linear polarized 532 nm Nd:Yag laser was employed with a 20 mW laser power and 0.1 s exposure time. The cross-sections for image acquisition were aligned beforehand with the radial direction parallel to the laser polarization Raman scattered light was detected using a back-illuminated charge-coupled device (CCD) camera, air-cooled with Peltier cooling to -60 °C, and a 600 g/mm grating, resulting in a spectral resolution of 3.8 cm^{-1}. The images were obtained with a lateral spatial resolution of approximately 0.3 µm, which is the diffraction limit.

The Raman scattering data analysis was performed in MATLAB and involved several pre-processing steps. First, each image was cropped to reduce the dataset size while keeping a full cross-section of a tracheid in view. Then, wavenumber ranges that did not contain any information on the specimens were removed, i.e., the wavenumbers below 300 cm^{-1} and above 3720 cm^{-1} approximately. Cosmic rays were eliminated through median filtering using the MATLAB built-in function medfilt1 with default settings. Next, an Alternating Least Squares (ALS) baseline correction was performed using parameters $\lambda = 10^5$ and $p = 0.005$ according to Eilers (2003) to reduce fluorescence contribution to the spectra (De Juan et al. 2014). Each image was clustered into two segments by use of k-means cluster analysis, which separated the lumina from the rest of the wood structure (i.e., the cell walls of tracheids and ray cells as well as the middle lamellae between cells, henceforth together denoted 'the cell wall cluster'). Before applying the k-means algorithm, the spectra were normalized to equal length using 2-norm. We found that this improved clustering based on visual inspection. For the spectra assigned to the cell wall cluster, average spectra were computed, and Raman peak heights or areas were estimated using a linear baseline that was individually set for each Raman band. Peak areas were preferred over peak heights when the peak of interest was an isolated peak and not a shoulder. The average spectra of cell walls were further baseline corrected (ALS, $\lambda = 10^4$ and $p = 0.001$) to enhance visual comprehension. The peak heights and areas were normalized over the aromatic ring stretching peak height at 1601 cm^{-1} to account for the differences in band intensity resulting from changes in the focal plane. Before normalization, peak areas lower than 0.1 and peak heights lower than 0.01 were respectively set to 0.1 and 0.01 to discard outliers. As in Ponzecchi et al. (2022), a statistical test was conducted to exclude unreliable information from the main peaks of interest, namely the C = O, O-D, and O-H stretching vibrations, due to high noise content. Furthermore, threshold clustering was utilized to identify the regions of the cell wall where hyphae or oxalate deposits were present. The spectra for which the sum of the peak areas at 641 cm^{-1} and 1457 cm^{-1} was higher than a certain threshold were assigned to oxalates. The threshold was individually set for each image in which hyphae were observed. The threshold ranged between 9 a.u. and 11 a.u. (arbitrary unit). The spectra assigned to the hyphae were clustered using k-means algorithm, baselined using normalized to equal length using 2-norm, baselined using ALS baseline correction with parameters $\lambda = 10^5$ and $p = 0.001$ and then over the peak height at 2938 cm^{-1}, to allow for visual comparison of intensities among spectra from different clusters. A summary of the peaks studied is provided in Table S2.

Results and discussion

Fungal degradation as seen on specimen level

Mass loss vs. harvest time

Figure 1 shows that no type of acetylation fully prevented decay. As expected, the UNTREATED wood had the lowest decay resistance, and its mass loss increased linearly during the first six weeks. UNIFORM HIGH wood had the highest decay resistance, while UNIFORM LOW and INTERFACE wood had lower resistance due to milder modification, which aligns with previous research by Beck et al. (2018) and Thygesen et al. (2021). The durability of the treated samples was influenced by the degree of acetylation, but the distribution of acetylation (uniform or interface) did not have a significant effect on durability. A slightly lower mass loss of UNIFORM LOW wood compared to INTERFACE wood was found and attributed to the higher R_{mod} of the UNIFORM LOW

wood (Table 1). That INTERFACE wood contains regions of untreated wood beneath the surfaces that are easily accessible for depolymerisation by the fungus also contributed to this result.

As expected from earlier studies, the mass loss varied substantially between replicates, confirming that several replicates are needed for this type of experiment. The spread in mass loss was higher for INTERFACE than for UNIFORM LOW. The reason is hypothesized to be the difference in distribution of acetylation within the cell wall, i.e., that slight variations in the INTERFACE modification directly will affect the fungal colonisation and depolymerisation more than slight variations in the UNIFORM LOW modification. Further, the spread in mass loss between the acetylated specimens increased with time, which might be due to uneven treatment, which becomes more decisive with increasing mass loss (Ringman et al. 2016).

Many samples showed negative mass losses. This is expected to be due to the fact that a mass loss will not show until the decrease in mass due to degradation becomes larger than the increase in fungal biomass (Ringman et al. 2016).

The fact that interface acetylated wood does not exhibit increased durability compared to uniformly acetylated wood, even at comparable levels of modification, suggests that the acetylated interface did not function as a significant barrier. Fungal access to the S2 layer may instead take place from the cell corner and middle lamella side via pits. This would align with previous observations (Füchtner and Thygesen 2023; Kim et al. 2015), and suggest that pits are likely access points, albeit hyphal penetration of the S3 layer from the lumen side has also been observed (Daniel 2016).

Since our imaging did not specifically focus on pits, we cannot confirm the observation of hyphae accessing the cell corners and middle lamella through these structures. In the Raman images obtained, hyphae were frequently found attached to the cell wall from the lumen side without any penetration (see Sect. 3.3).

Chitin monomer content vs. mass loss

Based on Fig. 2, it appears that the chitin monomer content in degraded wood samples is influenced by both the degree of decay and the degree of acetylation. The UNIFORM HIGH samples have a higher chitin monomer content for a given mass loss, which could be due to their longer exposure time to the fungus. However, a poor correlation between harvest time and chitin monomer content is shown in Fig. S1. Instead, it seems that acetylated samples have a higher chitin monomer content at similar mass loss compared to untreated wood. This could mean that the fungus needed to grow more hyphae to explore larger parts of the specimen in order to find suitable entryways into the wood with areas of sufficiently digestible material. This finding agrees with the more abundant mycelium growth observed on Norway spruce heartwood than on extracted Norway spruce

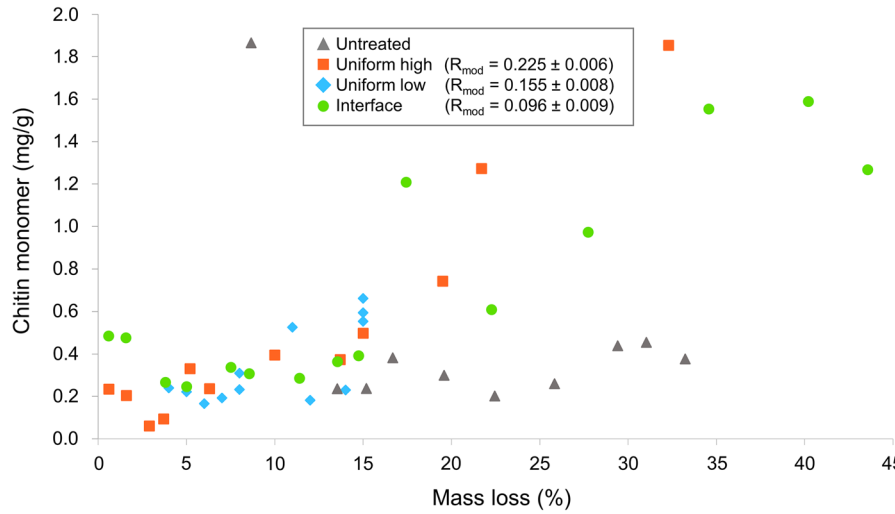

Fig. 2 Chitin monomer content (mg/g) plotted against the mass loss (%) of selected samples

heartwood when both types of wood were exposed to *Rhodonia placenta* (Füchtner and Thygesen 2023).

Cell wall changes in degraded samples

Deacetylation and carbohydrate degradation

The ATR-FTIR results were compared with previous studies to confirm the expected patterns of degradation. Based on earlier studies of similar specimens (Beck et al. 2018b; Thygesen et al. 2021), we chose to focus on the three bands at 1108, 1508 and 1732 cm^{-1}. The intensity ratio of the infrared bands at 1508 cm^{-1} to 1108 cm^{-1} increased in all types of wood as degradation progressed (Fig. 3a), confirming the more pronounced degradation of carbohydrates compared to lignin, as expected for a brown rot fungus (Beck et al. 2018b; Daniel 2016; Thygesen et al. 2021). In the degraded samples, less pronounced results were observed for the UNIFORM LOW samples. However, these results followed the same trend as the other types of acetylation, indicating both de-acetylation and carbohydrate degradation.

The ratio of the infrared bands at 1732 cm^{-1} to 1508 cm^{-1} significantly decreased in all degraded samples (Fig. 3b), indicating de-acetylation of the cell wall. This observation was seen in both acetylated and untreated samples and is in agreement with previous results (Beck et al. 2018). The de-acetylation of the cell wall was due to the action of the brown rot fungus, which both reduced the naturally occurring acetyl esters and those introduced by chemical modification (Khodayari et al. 2021; Terrett et al. 2019). The infrared analysis did not highlight any significant structural differences between the undegraded INTERFACE and UNIFORM samples. This is not surprising as the method gives information with lower spatial resolution than the thickness of the acetylated layers at the wood cell wall-lumen interface.

Figure 3c shows the infrared spectra from UNIFORM HIGH and UNTREATED samples plotted in the region between 800 and 1800 cm^{-1}, both from undegraded and degraded specimens. The plot shows that several bands were influenced by acetylation, while others seemed to decrease with degradation.

The unexamined absorbance bands in Fig. 3 include several peaks that are more intense in acetylated wood, such as the peaks around 1218 cm^{-1} and 1367 cm^{-1}. The difference in intensity between untreated and acetylated samples around those peaks is documented in previous studies and respectively linked to C=O stretch and to C−H bending of methoxyl groups (Faix 1991; Schwanninger et al. 2004; Thygesen et al. 2021). The peaks around 896 cm^{-1} and 1030 cm^{-1} are related to both carbohydrates and lignin. The former is linked to C_1−H deformation, while the latter is associated with C−H in-plane deformation and unconjugated C=O stretch (Schwanninger et al. 2004).

The results confirm that brown rot degraded the wood as expected from earlier studies, allowing further exploration of the chemical changes in even smaller detail with Raman.

Chemical changes of single wood cell walls after brown rot degradation

The average Raman spectra of the cell walls of a single wood tracheid in each wood cross-section were analysed. To compare the changes before and after degradation, the average cell wall spectra were normalized relative to the 1601 cm^{-1} peak height, which is associated with the stretching of aryl groups of lignin substructures and therefore is not susceptible to substantial brown rot degradation (Beck et al. 2018c; Daniel 2016; Thygesen et al. 2021). Each spectrum depicted in Fig. 4 is the average Raman spectrum from the cell walls of six tracheids. The results in Fig. 4 confirmed the de-acetylation and degradation of carbohydrates shown by the ATR-FTIR measurements, and indicated degradation of aliphatic lignin structures.

Brown rot fungi lack the enzymes to cleave the phenyl ring of lignin substructures, but they are capable of breaking down the aliphatic tail of the lignin structures, which is reflected in a loss of intensity of the 1660 cm^{-1} peak (Fig. 4) (Goodell et al. 2017; Yelle et al. 2011). Unfortunately, due to the normalization to the 1601 cm^{-1} peak, it is not possible to address any variation in total lignin intensity. Thus, it cannot be ruled out that even the aromatic lignin peak at 1601 cm^{-1} is affected by minor changes in absolute intensity, as recently suggested by Füchtner and Thygesen (2023).

De-acetylation was seen for all peaks associated with acetyl content, including 641 cm^{-1}, 912 cm^{-1}, 1740 cm^{-1}, and 2942 cm^{-1} (Fig. 4). Although the

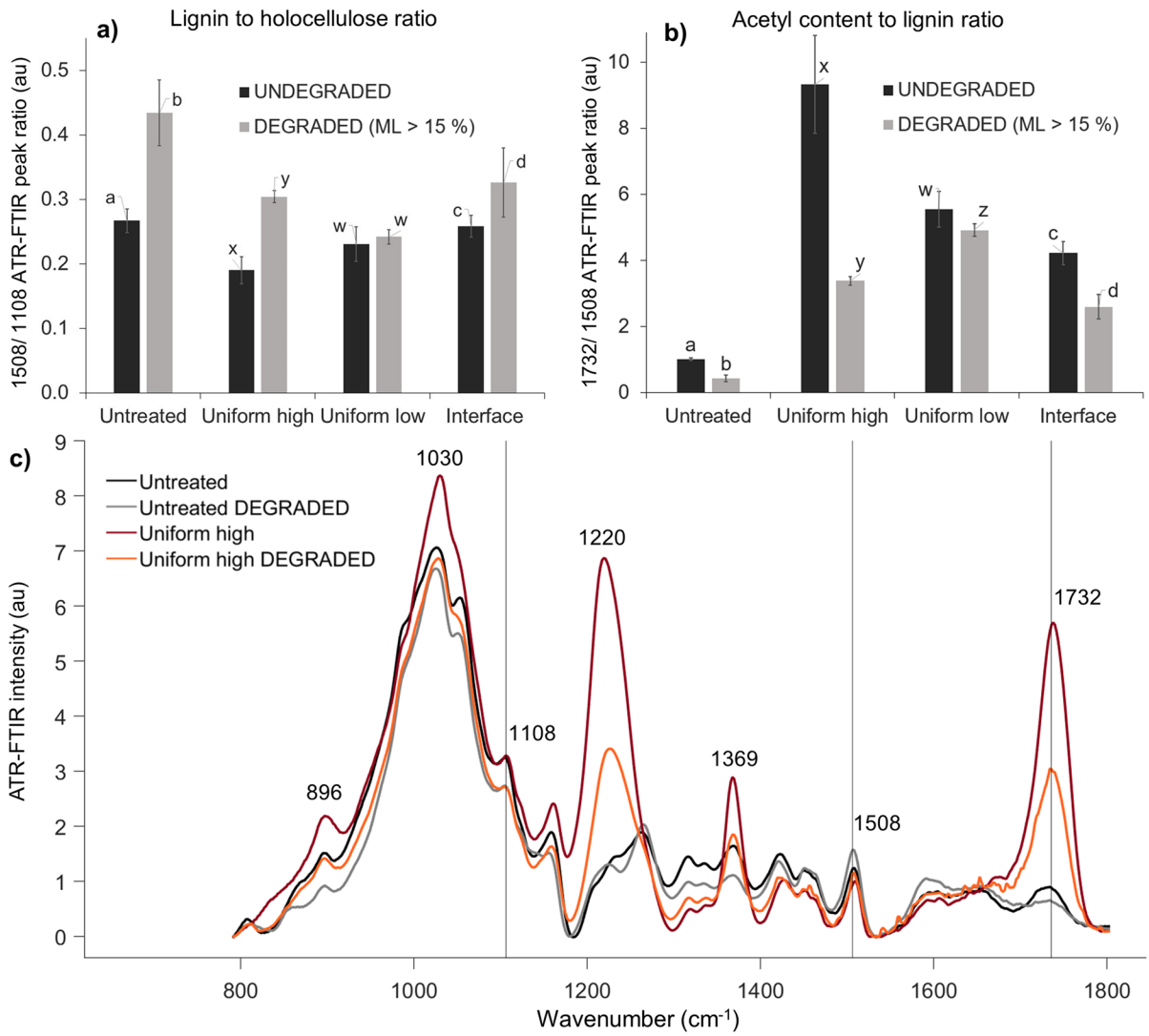

Fig. 3 Chemical changes due to degradation seen by ATR-FTIR for all types of wood studied, comprising **a** 1508/1108 ratio, **b** 1732/1508 ratio and **c** spectra of UNTREATED and UNIFORM HIGH wood samples, before and after degradation, in the selected wavenumber between 800 and 1800 cm^{-1}. Letters in (a) and (b) indicate significant difference ($p < 0.05$) tested with Wilcoxon rank-sum test

effect was less visible in untreated samples, it was still present in the average spectrum (Fig. S2).

Degradation of carbohydrates was observed at 1098 cm^{-1} and 1128 cm^{-1} for all types of wood studied and was also visible at 912 cm^{-1} and 2898 cm^{-1} in acetylated samples (Fig. 4), although here the information from acetylation or other lignin substructures may overlap (Bock and Gierlinger 2019; Digaitis et al. 2021). The peak at 2898 cm^{-1} could also be affected by the presence of hyphae in the cell walls (Füchtner et al. 2023).

In addition, the O−D peak at 2300–2685 cm^{-1} generally increased with degradation, indicating that the moisture content and accessible hydroxyls increased with degradation (Fig. 4). Simultaneously, an overall decrease in the O-H peak at 3170–3650 cm^{-1} confirm increased hydroxyl accessibility (Fig. 4).

Among the various wavenumbers analysed, only three showed an increase in intensity: 641 cm^{-1},

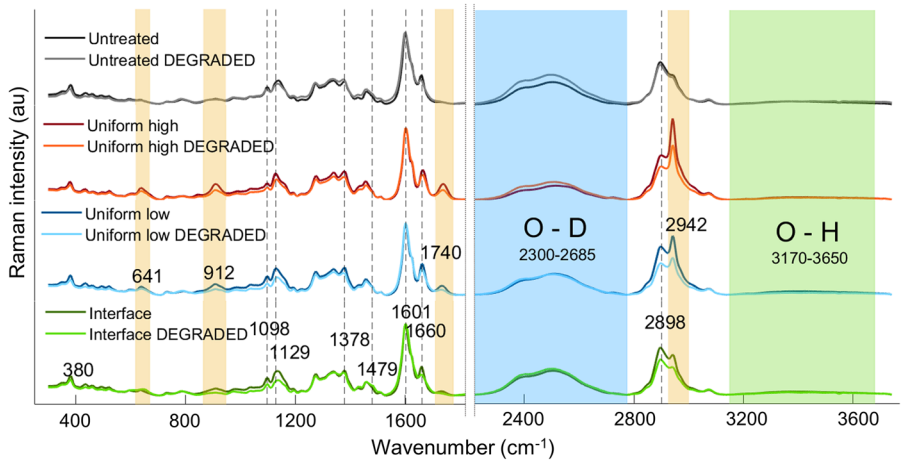

Fig. 4 Average Raman spectra of spruce cell walls before and after brow-rot degradation. UNTREATED in black and grey; UNIFORM HIGH in red and orange; UNIFORM LOW in blue and light blue; INTERFACE in green and light green. Bands in yellow are associated with acetylation; band in blue is O−D stretching, associated with moisture content and deuterated hydroxyl groups; band in green is O−H stretching, associated with inaccessible hydroxyl groups

1479 cm^{-1}, and 1379 cm^{-1}. A probable reason for changes in the first two bands is the formation of iron and calcium oxalates during degradation, caused by fungal oxidative activity (Füchtner et al. 2023). The third wavenumber, 1379 cm^{-1}, could likely be from the hydration with deuterium oxide of highly amorphous cell wall carbohydrates, possibly released in the cell wall by degradation (Agarwal 2022).

Bar charts displaying the average variations of all the studied Raman peaks before and after degradation can be found in Fig. S2.

Pattern of brown rot degradation at the sub-micron scale

A visualization of the sub-micron chemical changes before and after degradation can be seen by the Raman intensity maps of the cell walls (Fig. 5). These maps allow the visualization of specific chemical changes within the single cell walls of tracheids, otherwise imperceptible from the average spectra in Fig. 4. In addition to the de-acetylation and degradation trend of carbohydrates described before, the Raman intensity maps in Fig. 5 localize the sub-micron scale degradation pattern specific to components and types of wood acetylation.

As expected, the maps for the C=O peak (1740 cm^{-1}) (Fig. 5, first column) show that the acetyl content of UNTREATED wood was rather low in content and uniformly distributed in the cell walls, while acetyl groups mostly concentrated around the lumen in INTERFACE wood. The intensity maps of the C=O peak indicate that the cell wall undergoes de-acetylation during degradation, regardless of the type of wood attacked.

The holocellulose intensity maps (1130 cm^{-1}) (Fig. 5, second column) show carbohydrate degradation in the secondary cell wall of UNTREATED degraded samples, with slightly more prevalence in the radial direction than the tangential direction and in the proximity of the lumen. This effect could be due to the sample orientation relative to the laser polarization as well as to sample preparation. In acetylated samples, carbohydrates were degraded mostly in the secondary cell wall region which shows less acetylation, suggesting that acetylation locally protected holocellulose from degradation (Fig. 5, second column, white arrows). This trend was seen in several of the INTERFACE degraded samples, but also in the intensity maps of UNIFORM degraded samples (Fig. S3–S6). This implies that the acetylated "barrier" lining the lumen did not protect the untreated S2 layer from degradation.

The C−H intensity maps (2898 cm^{-1}) closely resembled the holocellulose intensity maps, with the exception of some clusters with higher signal intensity usually located in the cell wall-lumen interface of degraded samples (Fig. 5, third column). These

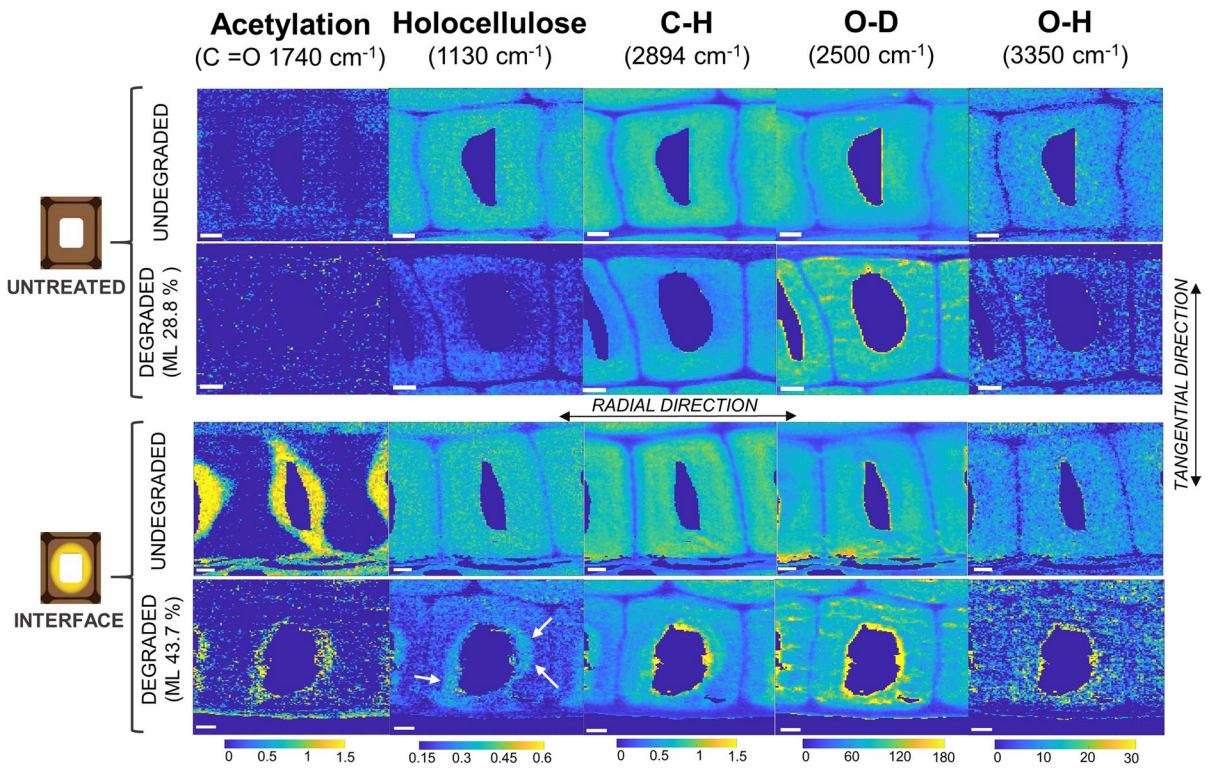

Fig. 5 Raman microspectroscopy intensity maps of untreated (UNTREATED) and interface acetylated wood (INTERFACE), both in pristine state and after brown rot degradation. Each column contains intensity maps of different cell wall tracheids, describe the same band and share common colour bar limits. Each map shows the composition of the cell wall cluster, while spectra assigned to the lumen cluster were artificially set to zero. The arrows point to the holocellulose which was protected by interface acetylation. The white scale bar in the images corresponds to 5 µm. Additional maps are available in Fig. S3–S6

clusters are likely due to the presence of fungal hyphae and will be further discussed in Sect. 3.3.

The O−D intensity map (2500 cm^{-1}) shows that the increased moisture content seen in the cell wall of degraded samples (Fig. 4) might be due to a formation of micro-pools of liquid water rather than a homogeneous increase in hygroscopicity (Fig. 5, fourth column). These pools have a thread-like shape and extend radially through the cell wall and travel through tracheids, crossing the less hygroscopic middle lamella. Interestingly, the O-D intensity maps did not resemble the one of holocellulose or C−H, because these pools were not confined to the most degraded region of the cell wall. Although a similar trend has been previously assigned to brown rot in degraded tracheids (Schwarze 2007), we believe that the origin of these threads is microcracks formed during sample preparation and cutting.

Finally, O−H intensity maps (Fig. 5, last column) are associated with inaccessible hydroxyls, known to be found in the most ordered areas of cellulose microfibrils (Hofstetter et al. 2006; Tarmian et al. 2017). These maps in UNTREATED wood showed similarity to the O−D map and the 1130 cm^{-1} map (holocellulose), both in pristine and degraded wood. The similarity with the holocellulose intensity maps (1130 cm^{-1}) is expected because fungi consume the cellulose, making some previously inaccessible hydroxyls groups accessible to water molecules while reducing the amount of carbohydrates. The consistent decrease in OH signal throughout the entire cell wall in acetylated and degraded samples, irrespective of the location of the acetylated region, coupled with the reduction in average signal from the peak at 380 cm^{-1}, suggests that degradation leads to a

reduction in cellulose crystallinity in both untreated and acetylated samples.

However, in INTERFACE, UNIFORM HIGH (Fig. 5) and UNIFORM LOW, holocellulose (1130 cm^{-1}) was partially protected after degradation in those regions where higher acetylation was present, but this was not reflected in O−H maps as in UNTREATED wood (Fig. S3–S6). Because of this ambiguity, while we can affirm that holocellulose was partly protected by acetylation, we cannot state that cellulose crystallinity was also preserved in those areas.

In this study, a preferential degradation of regions of the cell wall with lower acetylation was observed, while cell wall de-acetylation was often more pronounced in the outer edges of the S2 layer. These findings align with previous research by Füchtner and Thygesen (2023) on extracted and non-extracted Norway spruce heartwood, where brown rot degradation initiated in the S1 layer or compound middle lamella. However, while the presence of extractives delayed the initial stages of degradation, particularly the modification and breakdown of lignin-rich polymers, acetylation, even at late stage of degradation (ML > 15%), slowed the decay by locally protecting carbohydrates from degradation.

Overall, the combined outcome of macroscopic and microscopic investigations on the two different types of acetylation, i.e. INTERFACE and UNIFORM, suggest that while the these two types of acetylation affect where brown rot degradation takes place within the cell wall, both offer increased durability compared to native wood, and that at bulk level, this protection depends on the degree of modification rather than on the distribution of the treatment within the cell wall. From a commercial standpoint, this insight could signify a suggestion towards prioritizing the degree of modification.

Hyphae and extracellular polymeric substance

While analyzing the Raman images of degraded cell wall tracheids, it was found that twelve of them had small regions where the spectra were significantly different from the average cell wall spectrum. These regions contained spectra that could be grouped into three clusters.

Two of the three closely matched a reference hyphae of *R. placenta* (Füchtner et al. 2023), while the third resembled hydrated cell wall fragments such as lignin substructures and amorphous cellulose, or hydrated minerals such as calcium oxalates (Fig. 6, Fig. S7). Several of these groups were observed at the cell wall-lumen interface of degraded samples and had the two hyphae-looking spectra spatially divided into an inner and outer shell, as depicted in Fig. 6a−c and in Fig. S7.

In Fig. 6d, it was observed that the two concentric clusters had similar spectral features, particularly in the 1000–1400 cm^{-1} area, which was also consistent with the reference hyphae spectrum. The findings indicate that the hyphae involved in wood degradation look similar to the ones observed by Op De Beeck (2020) using OPTIR microspectroscopy. Hyphae are enveloped by an extracellular polymeric substance (EPS), which is a complex mixture of biopolymers. Here, we tentatively denote the inner cluster (Fig. 6, red) as the hyphae, while the outer cluster (Fig. 6, blue) is referred to as the EPS.

The hyphae showed lower O−D signal in the region between 2300 and 2700 cm^{-1} and higher O−H signal in the region between 3200 and 3650 cm^{-1} than the EPS (Fig. S7p). This suggest that the outer area of the hyphae is relatively richer in water and in inaccessible O−H groups, possibly from the chitin present in cell wall or from hydrated minerals such as oxalates. In addition, the spectrum of the hyphae showed a relatively stronger and broader peak in the region around 600–650 cm^{-1} (Fig. 6d) than the one of EPS. That band can be assigned to O−C=O in plane stretching, i.e. acetyl esters, chitin hydrogen bonding, or to ferrous/ferric chelated ions (Adebajo et al. 2006; Conde-Morales et al., 2020; De Gussem 2007). The two latter options are more likely as it is known that hyphae contain chitin as well as iron chelating elements in their cell walls, such as siderophores (Liu et al. 2013; Op De Beeck et al. 2021; Renshaw et al. 2002; Wagner et al. 2015). Further, iron is a key element in the Fenton chemistry employed by brown rot fungi to oxidatively degrade wood cell walls (Goodell et al. 2017; Hastrup et al. 2014; Op De Beeck et al. 2021; Tamaru et al. 2019). This is to our knowledge the first study to show the presence of chelated iron ions in the hyphae of wood-degrading fungi with vibrational spectroscopy, and this finding will need further investigations to be confirmed.

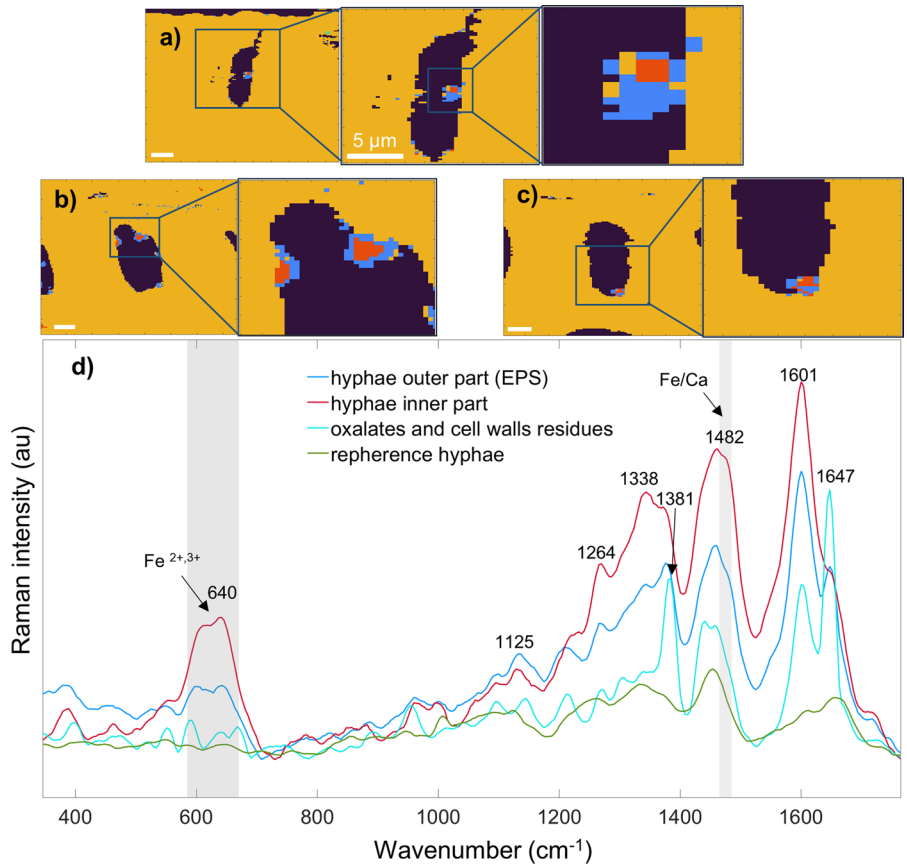

Fig. 6 **a–c** Cluster maps of Norway spruce cell wall cross-sections after brown rot degradation showing cell wall material in mustard colour, lumen in dark blue, while red and blue spectra show the hypothesized hyphae. **d** Raman spectra of the cluster tentatively assigned to hyphae cell wall and the extracellular polymeric matrix (EPS), and a reference Raman spectrum of hyphae from *Rhodonia placenta* (Füchtner et al. 2023), plotted in the wavenumber region between 320 cm^{-1} and 1780 cm^{-1}. The spectra in **d**) are normalized over the 2938 cm^{-1} peak height to allow relative comparison among them. The grey bands indicate the regions of the spectra where chelated metals and oxalates are expected to be found

In Fig. 6d, a strong shoulder peak can be observed at around 1483 cm^{-1} in both the EPS and the hyphae, but not in the reference Raman spectrum of a hyphae. This peak may be related to calcium oxalates or calcium chelated ions, which are known to be involved in brown rot wood cell wall degradation (Füchtner et al. 2023; Gadd 1999; Hastrup et al. 2014; Rusakov et al. 2021). While the reasoning behind the chelated calcium ions is analogous to the one of iron ions (Hastrup et al. 2014), calcium oxalates such as whewellite and weddellite are known byproducts of fungal degradation of wood cell walls (Connolly et al. 1996; Füchtner et al. 2023; Gadd et al. 2014; Armbruster and Danisi 2016; Rusakov et al. 2021). However, calcium oxalates have been observed in crystal forms only outside the hyphae, and to our knowledge they have never been reported to form inside hyphae or within their cell walls (Connolly et al. 1996; Füchtner et al. 2023; Gadd et al. 2014; Rusakov et al. 2021). Since the analysed samples are wood cross-sections, we assume that the concentric clusters show cross-sections of hyphal cell walls, but we cannot confirm this. Smearing of loose oxides over the sample surface during microtoming is also a possibility.

Another difference between the reference hyphae and the clustered hyphae spectra is the presence of two peaks around 1601 cm^{-1}. These peaks are distinct and located at 1593 cm^{-1} and 1604 cm^{-1} (raw spectra, not shown). In wood cell walls the peak at 1600 cm^{-1} is assigned to pure lignin components and originate from symmetric, aromatic C=C stretch of aromatic lignin substructures, so these peaks are likely to be signals from either lignin substructures or other phenolic compounds such as quinones, which contain aromatic rings like lignin (Agarwal and Atalla 2010; Bock et al. 2020; Gierlinger et al. 2013; Op De Beeck et al. 2021). Both aromatic lignin substructures and quinones are elements that can be found in the presence of wood and cell wall-degrading hyphae (Op De Beeck et al. 2021; Tamaru et al. 2019). Other than being a wood structural component, lignin substructures can function as electron donors for ferric iron,

possibly playing a key role in the chelated Fenton chemistry (Op De Beeck et al. 2020; Tamaru et al. 2019). Similarly, quinones, present in the EPS, could be involved in the redox cycling of iron and oxygen species, although this has not been verified (Op De Beeck et al. 2021). The prominent peak at 1647 cm^{-1} can also be attributed to lignin substructures and quinones (Agarwal 2009; Bock 2020).

We speculate that the differences observed between the spectra of the hyphae in the degraded cell wall, i.e., the hyphae and the EPS, and the reference hyphae might be due to differences in the substrate. The reference spectrum was from a hypha grown on soil, while the hypha from our material grew on wood. Differences in substrate composition can greatly impact fungal metal chelation and mineral formation (Connolly et al. 1996; Frank-Kamenetskaya et al. 2021; Hastrup et al. 2014; Heim et al. 2017; Op De Beeck et al. 2021).

The findings suggest a complex interplay between hyphae, metal ions, and degradation processes within the cell wall, highlighting the dynamic nature of fungal wood degradation and the multifaceted roles played by various components in this intricate system. Further research is warranted to explore these mechanisms in greater detail.

Conclusion

This study set out to investigate the impact of the distribution of acetylation within the cell wall on brown rot fungal degradation. Since the mass loss in the fungal degradation experiments was related to the overall degree of modification (R_{mod}) rather than the type of modification (UNIFORM or INTERFACE), the results showed that the overall degree of modification is more important in determining durability than the specific distribution of acetylation within the cell wall. Nevertheless, spectroscopic analyses conducted during the later stages of degradation revealed that acetylated regions retained a higher concentration of holocellulose, which shows that degradation primarily took place in cell wall regions that were less acetylated. This finding demonstrates that interface acetylation can be harnessed as a valuable tool for customizing wood cell wall degradation, targeting specific regions with precision. In addition, the results showed that the fungus required more fungal biomass (i.e., fungal mycelium) to degrade acetylated wood compared to untreated wood.

On a separate note, the study offers a glimpse into the characterization of fungal hyphae residing within lumina. The results from Raman imaging show that these hyphae exhibit a distinct two-layer structure, each with its own chemical signature.

Acknowledgments The authors gratefully acknowledge Ramūnas Digaitis for developing the acetylation protocols and acetylating the samples, and Sophie Füchtner for providing and discussing the Raman spectra of *Rhodonia placenta* hyphae. In addition, Aase og Ejnar Danielsens Fond, SNS Nordic Forest Research, the Swedish Research Council FORMAS, and NIBIO knowledge development project "Harvested wood products" are gratefully acknowledged for funding.

Author contributions LGT, MF, GA proposed the initial idea, LGT and EET supervised the research. GA designed and conducted decay tests and chitin monomer content analysis. MF designed and conducted wood sample preparation and modification. AP, LGT and EET designed and AP conducted the spectroscopic experiments, materials preparation, and characterizations. AP drafted the manuscript, and all authors discussed the results and contributed to manuscript preparation.

Funding Open access funding provided by Copenhagen University. The research was funded by Aase og Ejnar Danielsens Fond, SNS Nordic Forest Research, the Swedish Research Council FORMAS (Grant no. 2018-00387), and NIBIO knowledge development project "Harvested wood products" (Grant no. 10313).

Data availability The raw data will be made available by the authors upon request and without undue reservation.

Declarations

Competing interests The authors declare no competing interests.

References

Adebajo MO, Frost RL, Kloprogge JT, Kokot S (2006) Raman spectroscopic investigation of acetylation of raw cotton. Spectrochim Acta Part A Mol Biomol Spectrosc 64(2):448–453. https://doi.org/10.1016/j.saa.2005.07.045

Agarwal UP (2009) Raman spectroscopic characterization of wood and pulp fibers. Charact Lignocellul Mater. https://doi.org/10.1002/9781444305425.ch2

Agarwal UP (2022) Beyond crystallinity: using Raman Spectroscopic methods to further define Aggregated/Supramolecular structure of cellulose. Front Energy Res 10(April):1–10. https://doi.org/10.3389/fenrg.2022.857621

Agarwal UP, Atalla RH (2010) Chapter 4: vibrational spectroscopy. In: Heitner C, Dimmel DR, Schmidt JA (eds) Lignin and Lignans: advances in Chemistry, 1st edn. CRC Press, pp 104–136

Arantes V, Goodell B (2014) Current understanding of brown-rot fungal biodegradation mechanisms: a review. ACS Symp Ser 1158:3–21. https://doi.org/10.1021/bk-2014-1158.ch001

Arantes V, Milagres AMF, Filley TR, Goodell B (2011) Lignocellulosic polysaccharides and lignin degradation by wood decay fungi: the relevance of nonenzymatic Fenton-based reactions. J Ind Microbiol Biotechnol 38(4):541–555. https://doi.org/10.1007/s10295-010-0798-2

Armbruster T, Danisi R (2016) Highlights in mineralogical crystallography. De Gruyter (O), Berlin, München, Boston. https://doi.org/10.1515/9783110417104

Beck G, Hegnar OA, Fossdal CG, Alfredsen G (2018) Acetylation of Pinus radiata delays hydrolytic depolymerisation by the brown-rot fungus rhondonia placenta. Int Biodeterior Biodegrad 135(1431):39–52. https://doi.org/10.1016/j.ibiod.2018.09.003

Beck G, Thybring EE, Thygesen LG (2018) Brown-rot fungal degradation and de-acetylation of acetylated wood. Int Biodeterior Biodegrad 135(1431):62–70. https://doi.org/10.1016/j.ibiod.2018.09.009

Beck G, Thybring EE, Thygesen LG, Hill C (2018) Characterization of moisture in acetylated and propionylated radiata pine using low-field nuclear magnetic resonance (LFNMR) relaxometry. Holzforschung 72(3):225–233. https://doi.org/10.1515/hf-2017-0072

Bock P (2020) The vibrations of lignin: a discussion of the IR and Raman spectra of G-lignins and model compounds. Doctoral thesis. Universität für Bodenkultur, Wien

Bock P, Gierlinger N (2019) Infrared and Raman spectra of lignin substructures: coniferyl alcohol, abietin, and coniferyl aldehyde. J Raman Spectrosc 50(6):778–792. https://doi.org/10.1002/jrs.5588

Bock P, Nousiainen P, Elder T, Blaukopf M, Amer H, Zirbs R, Potthast A, Gierlinger N (2020) Infrared and Raman spectra of lignin substructures: Dibenzodioxocin. J Raman Spectrosc 51(3):422–431. https://doi.org/10.1002/jrs.5808

CEN (1997) Wood preservatives. Accelerated ageing of treated wood prior to biological testing. In: Leaching procedure. CEN-EN, vol 84. European Committee for Standardization (CEN), Brussels, Belgium

Conde-morales II, Hinojosa-reyes L, Guzmán-mar JL, Hernández-ramírez A, Sáenz-tavera IC, Villanueva-rodríguez M (2020) *Different Iron Oxalate sources as catalysts on Pyrazinamide Degradation by the photo-Fenton process at different pH values*

Connolly JH, Arnott HJ, Jellison J (1996) Patterns of calcium oxalate crystal production by three species of wood decay fungi. Scanning Microsc 10(2):385–400

Daniel G (2016) Fungal degradation of Wood cell walls. In: Kim YS, Funada R, Singh AP (eds) Secondary Xylem Biology: origins functions, and applications. Elsevier Inc, Amsterdam. https://doi.org/10.1016/B978-0-12-802185-9.00008-5

De Gussem K (2007) Optimisation of Raman spectroscopy for the analysis of Basidiomycota: spores, latex and mycelium. Thesis. https://doi.org/10.13140/RG.2.1.1646.4484.

De Juan A, Piqueras S, Maeder M, Hancewicz T, Duponchel L, Tauler R (2014) Chemometric tools for image analysis. Infrared and Raman spectroscopic imaging, 2nd edn. Wiley, Hoboken, pp 57–110

De Op M, Troein C, Siregar S, Gentile L, Abbondanza G, Peterson C, Persson P, Tunlid A (2020) Regulation of fungal decomposition at single-cell level. ISME J 14(4):896–905. https://doi.org/10.1038/s41396-019-0583-9

Digaitis R, Thybring EE, Thygesen LG, Fredriksson M (2021) Targeted acetylation of wood: a tool for tuning wood-water interactions. Cellulose 28(12):8009–8025. https://doi.org/10.1007/s10570-021-04033-z

Durmaz S, Özgenç Ö, Boyaci IH, YIldIz ÜC, Erişir E (2016) Examination of the chemical changes in spruce wood degraded by brown-rot fungi using FT-IR and FT-Raman spectroscopy. Vib Spectrosc 85:202–207. https://doi.org/10.1016/j.vibspec.2016.04.020

Eikenes M, Fongen M, Roed L, Stenstrøm Y (2005) Determination of chitosan in wood and water samples by acidic hydrolysis and liquid chromatography with online fluorescence derivatization. Carbohydr Polym 61(1):29–38. https://doi.org/10.1016/j.carbpol.2005.02.006

Eilers PHC (2003) Baseline correction with asymmetric least squares smoothing. Anal Chem 75(14):3631–3636

Faix O (1991) Classification of Lignins from different Botanical origins by FT-IR Spectroscopy. Holzforschung 45(s1):21–28. https://doi.org/10.1515/hfsg.1991.45.s1.21

Frank-Kamenetskaya OV, Zelenskaya MS, Izatulina AR, Vereshchagin OS, Vlasov DY, Himelbrant DE, Pankin DV (2021) Copper oxalate formation by lichens and fungi. Sci Rep 11(1):1–9. https://doi.org/10.1038/s41598-021-03600-5

Fredriksson M, Wadsö L, Johansson P, Ulvcrona T (2016) Microclimate and moisture content profile measurements in rain exposed Norway spruce (Picea abies (L.) Karst.) Joints. Wood Mater Sci Eng 11(4):189–200. https://doi.org/10.1080/17480272.2014.965742

Füchtner S, Thygesen LG (2023) Subcellular level impact of extractives on brown rot decay of Norway spruce elucidated by confocal Raman microscopy and multivariate data analysis. Wood Science and Technology, vol 0123456789. Springer, Berlin Heidelberg. https://doi.org/10.1007/s00226-023-01476-4

Füchtner S, Alfredsen G, Thygesen LG (2023) Oxalate found in wood cell wall during incipient brown rot degradation.

Int Biodeterior Biodegrad 177(November 2022):105531. https://doi.org/10.1016/j.ibiod.2022.105531

Gadd GM (1999) Fungal production of citric and oxalic acid: Importance in metal speciation, physiology and biogeochemical processes. In *Advances in Microbial Physiology* (Vol. 41). Elsevier Masson SAS. https://doi.org/10.1016/s0065-2911(08)60165-4

Gadd GM, Bahri-Esfahani J, Li Q, Rhee YJ, Wei Z, Fomina M, Liang X (2014) Oxalate production by fungi: significance in geomycology, biodeterioration and bioremediation. Fungal Biol Rev 28(2–3):36–55. https://doi.org/10.1016/j.fbr.2014.05.001

Gierlinger N, Keplinger T, Harrington M (2012) Imaging of plant cell walls by confocal Raman microscopy. Nat Protoc 7(9):1694–1708. https://doi.org/10.1038/nprot.2012.092

Gierlinger N, Keplinger T, Harrington M, Schwanninger M (2013) Raman imaging of lignocellulosic feedstock. Cellul Biomass Convers. https://doi.org/10.5772/50878

Goodell B, Zhu Y, Kim S, Kafle K, Eastwood D, Daniel G, Jellison J, Yoshida M, Groom L, Pingali SV, O'Neill H (2017) Modification of the nanostructure of lignocellulose cell walls via a non-enzymatic lignocellulose deconstruction system in brown rot wood-decay fungi. Biotechnol Biofuels 10(1):1–15. https://doi.org/10.1186/s13068-017-0865-2

Guggiari M, Bloque R, Aragno M, Verrecchia E, Job D, Junier P (2011) Experimental calcium-oxalate crystal production and dissolution by selected wood-rot fungi. Int Biodeterior Biodegrad 65(6):803–809. https://doi.org/10.1016/j.ibiod.2011.02.012

Hastrup ACS, Jensen B, Jellison J (2014) Fungal accumulation of metals from building materials during brown rot wood decay. Arch Microbiol 196(8):565–574. https://doi.org/10.1007/s00203-014-0993-z

Heim C, Quéric NV, Ionescu D, Schäfer N, Reitner J (2017) Frutexites-like structures formed by iron oxidizing biofilms in the continental subsurface (Äspö Hard Rock Laboratory, Sweden). PLoS ONE 12(5):e0177542. https://doi.org/10.1371/journal.pone.0177542

Hill CAS (2006) Wood Modification: Chemical, Thermal and Other Processes. In *Wood Modification: Chemical, Thermal and Other Processes*. https://doi.org/10.1002/0470021748

Hofstetter K, Hinterstoisser B, Salmén L (2006) Moisture uptake in native cellulose - the roles of different hydrogen bonds: a dynamic FT-IR study using deuterium exchange. Cellulose 13(2):131–145. https://doi.org/10.1007/s10570-006-9055-2

Khodayari A, Thielemans W, Hirn U, Van Vuure AW, Seveno D (2021) Cellulose-hemicellulose interactions - a nanoscale view. Carbohydr Polym 270(April):118364. https://doi.org/10.1016/j.carbpol.2021.118364

Kim JS, Gao J, Daniel G (2015) Ultrastructure and immunocytochemistry of degradation in spruce and ash sapwood by the brown rot fungus postia placenta: characterization of incipient stages of decay and variation indecayprocess. Int Biodeterior Biodegradation 103:161–178. https://doi.org/10.1016/j.ibiod.2015.05.005

Liu X, Eusterhues K, Thieme J, Ciobota V, Höschen C, Mueller CW, Küsel K, Kögel-Knabner I, Rösch P, Popp J, Totsche KU (2013) STXM and NanoSIMS investigations on EPS fractions before and after adsorption to goethite. Environ Sci Technol 47(7):3158–3166. https://doi.org/10.1021/es3039505

Mantanis GI (2017) Chemical modification of Wood by Acetylation or Furfurylation: a review of the Present scaled-up technologies. BioResources 12(2):4478–4489. https://doi.org/10.15376/BIORES.12.2.MANTANIS

Mantanis GI, Young RA, Rowell RM (1994) Swelling of wood - part 1. Swelling in water. Wood Sci Technol 28(2):119–134. https://doi.org/10.1007/BF00192691

Op De Beeck M, Persson P, Tunlid A (2021) Fungal extracellular polymeric substance matrices – highly specialized microenvironments that allow fungi to control soil organic matter decomposition reactions. Soil Biol Biochem 159(March):108304. https://doi.org/10.1016/j.soilbio.2021.108304

Ponzecchi A, Thybring EE, Fredriksson M, Solsona SP, Thygesen LG (2022) Raman micro-spectroscopy of two types of acetylated Norway spruce wood at controlled relative humidity. Front Plant Sci. https://doi.org/10.3389/fpls.2022.986578

Renshaw JC, Robson GD, Trinci APJ, Wiebe MG, Livens FR, Collison D, Taylor RJ (2002) Fungal siderophores: structures, functions and applications. Mycol Res 106(10):1123–1142. https://doi.org/10.1017/S0953756202006548

Ringman R, Pilgård A, Kölle M, Brischke C, Richter K (2016) Effects of thermal modification on Postia placenta wood degradation dynamics: measurements of mass loss, structural integrity and gene expression. Wood Sci Technol 50(2):385–397. https://doi.org/10.1007/s00226-015-0791-z

Rowell RM (1983) Chemical Modification of Wood. In: Rowell RM (ed) Issue Handbook of Wood Chemistry and Wood Composites. CRC Press. https://doi.org/10.3139/9783446442504.022

Rusakov A, Kuz'mina M, Frank-Kamenetskaya O (2021) Biofilm medium chemistry and calcium oxalate morphogenesis. Molecules. https://doi.org/10.3390/molecules26165030

Schilling JS, Duncan SM, Presley GN, Filley TR, Jurgens JA, Blanchette RA (2013) Colocalizing incipient reactions in wood degraded by the brown rot fungus postia placenta. Int Biodeterior Biodegrad 83:56–62. https://doi.org/10.1016/j.ibiod.2013.04.006

Schultze-Dewitz G (1966) Beziehungen Zwischen Der Elastizität Und Der Statischen Sowie Dynamischen Biegefestigkeit Von Kiefernholz Nach dem Angriff durch echte holzzerstörende Pilze. Holz Als Roh Und Werkstoff 24(10):506–512. https://doi.org/10.1007/BF02612884

Schwanninger M, Rodrigues JC, Pereira H, Hinterstoisser B (2004) Effects of short-time vibratory ball milling on the shape of FT-IR spectra of wood and cellulose. Vib Spectrosc 36(1):23–40. https://doi.org/10.1016/j.vibspec.2004.02.003

Schwarze FWMR (2007) Wood decay under the microscope. Fungal Biol Rev 21(4):133–170. https://doi.org/10.1016/j.fbr.2007.09.001

Tamaru Y, Yoshida M, Eltis LD, Goodell B (2019) Multiple iron reduction by methoxylated phenolic lignin structures and the generation of reactive oxygen species by lignocellulose surfaces. Int J Biol Macromol 128:340–346. https://doi.org/10.1016/j.ijbiomac.2019.01.149

Tarmian A, Burgert I, Thybring EE (2017) Hydroxyl accessibility in wood by deuterium exchange and ATR-FTIR spectroscopy: methodological uncertainties. Wood Sci Technol 51(4):845–853. https://doi.org/10.1007/s00226-017-0922-9

Terrett OM, Lyczakowski JJ, Yu L, Iuga D, Franks WT, Brown SP, Dupree R, Dupree P (2019) Molecular architecture of softwood revealed by solid-state NMR. Nat Commun 10(1):1–11. https://doi.org/10.1038/s41467-019-12979-9

Thybring EE (2013) The decay resistance of modified wood influenced by moisture exclusion and swelling reduction. Int Biodeterior Biodegrad 82:87–95. https://doi.org/10.1016/j.ibiod.2013.02.004

Thygesen LG, Beck G, Nagy NE, Alfredsen G (2021) Cell wall changes during brown rot degradation of furfurylated and acetylated wood. Int Biodeterior Biodegrad 162:105257. https://doi.org/10.1016/j.ibiod.2021.105257

Wagner L, Bader TK, Ters T, Fackler K, De Borst K (2015) A combined view on composition, molecular structure, and micromechanics of fungal degraded softwood. Holzforschung 69(4):471–482. https://doi.org/10.1515/hf-2014-0023

Williams FC, Hale MD (2003) The resistance of wood chemically modified with isocyanates: the role of moisture content in decay suppression. Int Biodeterior Biodegrad 52(4):215–221. https://doi.org/10.1016/S0964-8305(03)00070-2

Yelle DJ, Wei D, Ralph J, Hammel KE (2011) Multidimensional NMR analysis reveals truncated lignin structures in wood decayed by the brown rot basidiomycete Postia placenta. Environ Microbiol 13(4):1091–1100. https://doi.org/10.1111/j.1462-2920.2010.02417.x

Zelinka SL, Altgen M, Emmerich L, Guigo N, Keplinger T, Kymäläinen M, Thybring EE, Thygesen LG (2022) Rev Wood Modif Wood Functionalization Technol. 1–46

Zhang J, Presley GN, Hammel KE, Ryu JS, Menke JR, Figueroa M, Hu D, Orr G, Schilling JS (2016) Localizing gene regulation reveals a staggered wood decay mechanism for the brown rot fungus postia placenta. Proc Natl Acad Sci USA 113(39):10968–10973. https://doi.org/10.1073/pnas.1608454113